Electrical and optical properties of porous nanocrystalline TiO2 films

ARTICLE *in* THE JOURNAL OF PHYSICAL CHEMISTRY · AUGUST 1995

Impact Factor: 2.78 · DOI: 10.1021/j100031a027

Electrical and Optical Properties of Porous Nanocrystalline TiO_2 Films

Fei Cao, Gerko Oskam, and Peter C. Searson*

Department of Materials Science and Engineering, The Johns Hopkins University, Baltimore, Maryland 21218

Jeremy M. Stipkala, Todd A. Heimer, Fereshteh Farzad, and Gerald J. Meyer*

Department of Chemistry, The Johns Hopkins University, Baltimore, Maryland 21218

Received: April 24, 1995[⊗]

The optical and electrochemical properties of nanocrystalline TiO_2 electrodes in acidic aqueous solution are reported. Cyclic voltammetry, UV/vis/NIR attenuance, EPR, photocurrent spectroscopy, and electrochemical impedance measurements are presented. At negative applied potentials the TiO_2 films turn black, and an EPR spectrum appears which we attribute to Ti(III) species. The results are described in terms of a model in which the reduction of TiO_2 leads to band edge unpinning.

Introduction

Recently, there has been increased interest in the photoelectrochemical properties of nanostructured materials.[1] This interest is derived from a variety of novel optical and electronic processes observed in these materials which are often not seen in bulk materials. An important class of nanostructured materials are porous nanocrystalline films. These materials can be easily fabricated by spin-coating colloidal solutions onto conductive substrates. These films provide a high surface area useful for device applications, and practical applications in water detoxification,[2] electrochromic devices,[3] and solar energy conversion[4−7] appear likely in the near future.

A major challenge in the development of this field is to better understand the potential distribution[8] and carrier transport mechanism(s)[9] in these materials. This is particularly difficult, however, due to the complex three-dimensional structure of the porous films. A significant theoretical contribution to the potential distribution problem in porous nanocrystalline TiO_2 films was recently reported by Rothenberger et al.[8] These workers employed a Schottky junction model to derive the potential distribution within the TiO_2 particles at negative applied potentials. The model is based on the supposition that an accumulation layer can be created within each nanocrystalline particle as the potential is shifted negative of the flat-band potential. More recently, this model has been applied to nanocrystalline TiO_2 films in operational electrochemical cells.[10] The observation of a black color and a blue shift in the apparent fundamental absorption edge at negative applied potentials was taken as evidence for accumulation layer formation. Analysis of the absorbance spectrum as a function of applied potential, along with several assumptions, allowed determination of the flat-band potential, U_{fb}. With this methodology, a shift in U_{fb} of 60 mV per pH unit was observed as is common for metal oxide semiconductor photoanodes.[11]

In order to evaluate the validity of this approach, it is necessary to verify the assumptions in the model. First, the application of Schottky junction models to colloidal materials is not straightforward, especially when the size of the particles is very small.[7,12] The colloidal dimensions severely restrict the extent of electric fields that a particle can support, and concepts such as depletion and accumulation may not be generally applicable.[7] However, as was demonstrated by Rothenberger et al.[8] and others,[13] an accumulation layer is thinner than a depletion layer when considering cases where the same amount of charge is transferred across the same interface. Therefore, in small semiconductor particles an appreciable accumulation layer may be more likely than a depletion layer. However, a strong case can be made that accumulation layer formation under steady state conditions at *any* semiconductor−electrolyte (SC/E) interface is unlikely. While accumulation layer formation is well documented in solid state devices, there are very few examples at SC/E interfaces. Because this is a central issue in this paper, it is worthwhile to briefly discuss this point in the context of pertinent literature results.

For an n-type semiconductor, as the Fermi level is raised toward the flat-band potential, large cathodic currents can flow as the surface electron concentration increases. This is the weak depletion condition often referred to as forward bias. The onset of cathodic currents has been reported for band bending (in depletion) as large as 600 mV.[14] At smaller band bending the cathodic currents can be very large (in excess of 10 mA/cm^2). In many cases the observation of cathodic currents at applied potentials negative to the flat-band potential, determined by Mott−Schottky analysis, is cited as evidence for accumulation. However, the determination of the position of the Fermi level with respect to the flat-band potential is problematic since the flat-band potential is not a singular parameter and is often dependent on the presence of electrically active surface states, adsorbates, reaction intermediates, etc. The position of the flat-band potential determined by extrapolation from the deep depletion condition (for example, Mott−Schottky analysis) does not imply that the band edges are fixed as the Fermi level is raised. The observation of large cathodic currents, therefore, is not indicative of an accumulation layer for the reasons described above.

In principle, capacitance measurements can be used to characterize an accumulation layer. The potential dependence of an accumulation layer capacitance is given by[15]

$$C_{SC} \propto \exp(-e\Delta\phi_{SC}/2kT) \quad (1)$$

Measurements of the capacitance at potentials close to the flat-band potential, however, are usually difficult due to the presence of large currents. Under these conditions the measured capacitance should be be corrected by the dissipation factor, which is significant at modest currents but is rarely reported in the literature. In addition, for moderately doped materials, the space

[⊗] Abstract published in *Advance ACS Abstracts,* July 1, 1995.

0022-3654/95/2099-11974$09.00/0

charge capacitance in accumulation is expected to be relatively large, and for $C_{SC} \geq C_H$, any change in the applied potential is expected to fall across the Helmholtz layer. To our knowledge, the 120 mV per decade dependence of C_{SC} predicted by eq 1 has not been reported.

Spectroscopic measurements can provide evidence for the formation of an accumulation layer. For example, the optical properties of electrons can provide information on the degree of electronic localization in the semiconductor. The molar absorptivity of a free moving electron increases with wavelength, where a trapped electron displays an absorption maximum.[16] A difficulty with this approach is that if the electron is trapped in a shallow level, the absorption maximum may be in the far-infrared where competitive absorption by the solvent or substrate makes detection difficult. Therefore, the observation of an increasing absorptivity in the visible and near-IR regions may lead to the false conclusion that free carriers are present, when in fact an absorption maximum is present at lower energies.

Band edge photoluminescence has also been given as evidence for accumulation.[17] A dramatic increase in the photoluminescence intensity from CdS and CdSe semiconductors biased negative of U_{fb} (determined by extrapolation from flat-band conditions) has been attributed to formation of an accumulation layer. While photoluminescence probes have been useful for mapping surface electric fields, observed changes in photoluminescence intensity with applied potential may result from surface recombination velocity changes and/or changes in the surface electric field.[18] Quantitating the relative contributions from these two factors is nontrivial. In addition, surface chemistry, corrosion, and/or hydrogen evolution accompany the observed photoluminescence intensity increase at negative potentials, making interpretation difficult.

Electroreflectance measurements have also been used to probe electric fields at the SC/E interface.[19] The observation of a change in sign of the reflectance signal has been interpreted as a change from depletion to accumulation, and the corresponding potential was taken as the flat-band potential. However, this technique is also sensitive to changes in surface chemistry, adsorption, and surface states so that assignment is not straightforward. The above spectroscopic techniques should therefore be regarded as indirect evidence for accumulation layer formation which is inconclusive in the absence of other supporting data.

The transient formation of an accumulation layer in low doped ZnO at liquid interfaces has been reported by Eger and Goldstein.[20] However, these authors clearly show that accumulation could not be maintained under dc conditions due to the cathodic current flow across the interface. Dewald[15] has pointed out that accumulation should only be possible with very low doped materials since at moderate dopant concentrations the surface quickly becomes degenerate, and any further increase in applied potential is dropped across the Helmholtz layer.

From the above discussion it is clear that even at single crystal materials, the demonstration of free electron concentrations greater than equilibrium values is very difficult. For porous nanocrystalline TiO_2 films, the situation is further complicated by the complex three-dimensional structure of the films and the small particle size, and it is, therefore, unlikely that conclusive evidence for accumulation layer formation will be forthcoming. What is more generally observed for an n-type semiconductor as the Fermi level is raised is "band edge unpinning", which is also referred to as "Fermi level pinning".[21] The basis for this model is that the presence of electrically active surface states, chemisorbed species, or reaction intermediates unpins the band edges so that any further increase in the applied potential is dropped across the Helmholtz layer and does not change the band bending. As will be shown later, large shifts in the band edges, >1.6 eV, can be induced by the filling and emptying of surface states. A large density of surface states is expected in porous nanocrystalline films as a result of the high surface area.

In this paper we report evidence that supports a band edge unpinning model for the potential distribution close to the flat-band potential in nanostructured TiO_2 films at pH 2. Cyclic voltammetry, photocurrent spectroscopy, UV/vis/NIR, EPR, and electrochemical impedance measurements are reported.

Experimental Section

Materials Preparation. The sample preparation largely followed the method reported by Grätzel and co-workers.[4c] A paste of TiO_2 powder (Degussa P-25, approximately 70% anatase and 30% rutile) in 4 mL of water containing 0.4 mL of acetylacetone to prevent reaggregation was diluted by the slow addition of 16 mL of water under continued grinding. Finally, 0.2 mL of surfactant (Triton X-100) was added to the suspension. Nanostructured TiO_2 electrodes were made in the following way. F-doped SnO_2 conducting glass (Libby Owens Ford, 8 Ω/square) was cut and cleaned with ethanol. The suspension was applied to the substrates masked with tape and air-dried for 15 min. After removing the mask, the sample was sintered in air for 30 min at 450 °C. Thicker films were obtained by repeating this process.

The thickness of the nanostructured TiO_2 electrodes was determined with a Tencor Alpha Step 200 profilometer. Transmission electron microscopy of the films was performed with a Phillips 420 microscope. In this case the TiO_2 suspension was applied directly to TEM grids and subsequently sintered using the conditions described above. X-ray diffraction was performed on a Phillips diffractometer using Cu Kα irradiation.

Electrochemistry. The electrochemistry was performed in a three-electrode cell with a platinum counter electrode and saturated sodium calomel reference electrode (SSCE). Unless otherwise stated, the geometric area of the TiO_2 electrode exposed to the electrolyte was 0.4 cm^2, and the electrolyte was 0.1 M Na_2SO_4 adjusted to pH 2 with H_2SO_4. Cyclic voltammetry was performed with a BAS CV-27 potentiostat. Electrode impedance measurements were made with a Solartron 1255 frequency response analyzer and a Solartron 1286 potentiostat.

Photocurrent Spectroscopy. Photocurrent action spectra were recorded in a three-electrode cell arrangement at pH 2 as described above. The TiO_2 photoanode was illuminated through the conducting glass support with a 450 W Xe lamp coupled to a SPEX 0.22 m monochromator. The incident irradiance was measured with a calibrated Si photodiode from UDT Technologies. An uncoated tin oxide electrode was placed in front of the photodiode to correct for competitive attenuance from the conducting glass support. The corrected photon-to-current efficiency (PCE) was calculated as previously described.[5]

Spectroscopy. Attenuance spectra were obtained on a Hewlett-Packard 8451A diode array and a Shimadzu UV 160U or a Cary 14 spectrophotometer. The reference sample was a TiO_2 film biased at 0.0 V (SSCE) or in some cases an uncoated conducting glass electrode.

Electron paramagnetic resonance (EPR) spectra were obtained with a Varian E-12 spectrometer operating at 8.6 GHz at 77 K. The g factors were calibrated by reference to a powder sample of 1,1-diphenyl-2-picrylhydrazyl (DPPH, $g = 2.0037 \pm 0.0002$).[22] EPR samples were prepared by electrochemically reducing TiO_2 films in a N_2-filled drybox at −1.2 V (SSCE) for 30 min in 0.1 M Na_2SO_4 at pH 2. The reduced TiO_2 particles were scraped

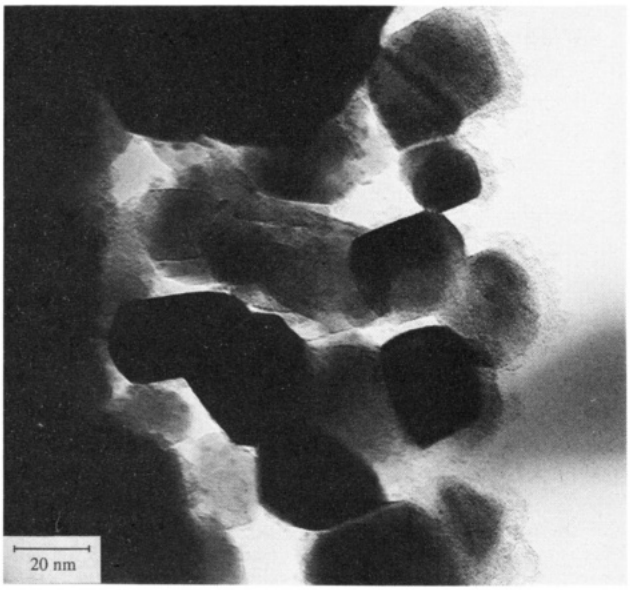

Figure 1. TEM micrograph of a colloidal suspension of TiO_2 prepared on a TEM grid and sintered at 450 °C for 15 min.

from the conducting glass support directly into quartz EPR tubes and sealed. The samples were stable in the absence of air for several months.

Results

Figure 1 displays a TEM micrograph of a sintered TiO_2 film prepared using the technique described above. Moire fringes can be seen where particles overlap, revealing the crystallinity of the particles. Electron diffraction measurements suggest that there are no structural differences between the powder and the sintered films. The Degussa P-25 material is approximately 70% anatase and 30% rutile. X-ray diffraction on the TiO_2 powder and the sintered films was similar with characteristic peaks associated with both anatase and rutile. These results also show that the transformation of anatase to rutile during the sintering process is not significant. The TiO_2 films are typically 16 μm thick as determined by profilometry measurements.

In analyzing UV−vis spectra from these porous nanocrystalline films, it is difficult to determine the relative contributions from absorption, scattering, and reflection. We therefore report these data as the attenuance, given by −log(transmittance).[23] The use of this quantity avoids assumptions concerning the reference material and potential-dependent scattering or reflectivity changes. If the changes in transmittance are solely due to changes in absorption, then attenuance is equal to absorption.

Figure 2a shows a plot of the attenuance versus wavelength for a TiO_2 film under open-circuit conditions in 0.1 M Na_2SO_4 at pH 2. This figure shows that the transmission from these films is low throughout most of the visible region. Experimentally, the high-energy limit for attenuance measurements is determined by fundamental absorption from the TiO_2 and at low energy by the tin oxide substrate where the transmission is less than 40% at 1500 nm. When placed in an operational photoelectrochemical cell in pH 2 aqueous solution, these films convert photons to electrons. Shown in Figure 2b is a plot of photon-to-current-efficiency versus wavelength, obtained at three different potentials and corrected for attenuance from the conducting glass support. In all cases the photoanodes were excited through the conductive tin oxide support, i.e., substrate side illumination.[9] The shape of the photoaction spectrum was qualitatively the same for all samples: a steep onset is observed

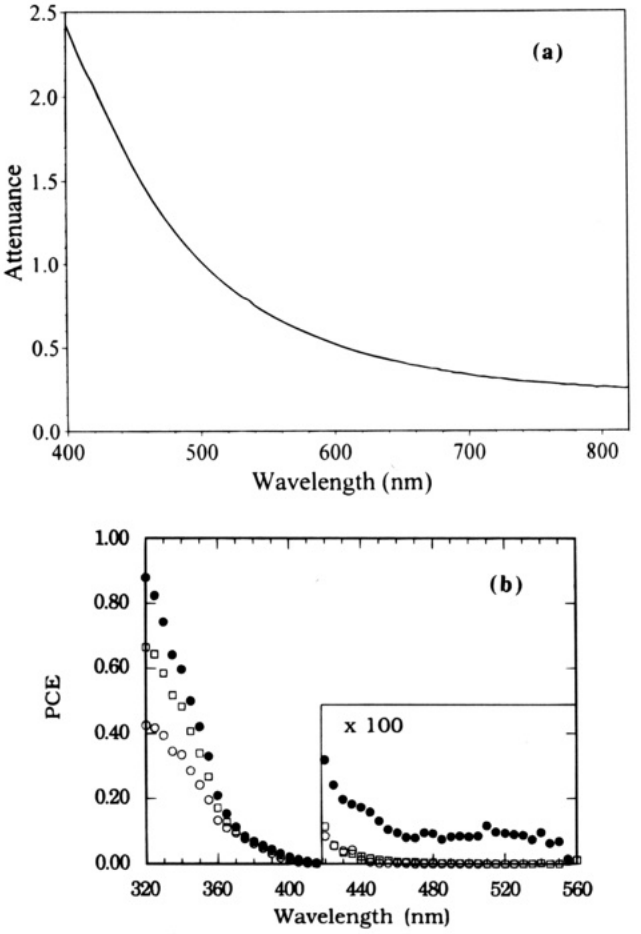

Figure 2. (a) Attenuance spectrum of a TiO_2 film under open-circuit conditions in 0.1 M Na_2SO_4 at pH 2. A pH 2 solution with 0.1 M Na_2SO_4 and a tin oxide electrode were used as the reference. Instrument resolution is ±2 nm and ±0.002 attenuance units. (b) Photoaction spectrum of a nanostructured TiO_2 electrode in 0.1 M Na_2SO_4 at pH 2, where PCE is the photon-to-current efficiency. The photocurrent was measured at 0.30 V (open circles), 0.50 V (squares), and 1.00 V (filled circles) versus an SSCE reference electrode. The inset is an expansion of the visible region.

at about 330−340 nm with a much smaller tail that extends out into the visible region. This tail is more clearly observed at positive applied potentials where the photocurrent is larger.

Application of a negative potential to the TiO_2 working electrode in a standard three-electrode arrangement results in a reductive current and the appearance of a uniform black color. No significant color change was detected for a conductive glass substrate in the same potential range. In 0.1 M Na_2SO_4 solution at pH 2 the visible attenuance begins to increase at about −0.4 V (SSCE). Attenuance spectra as a function of applied potential are shown in Figure 3, with a TiO_2 electrode biased at 0.0 V (SSCE) in the same solution as the reference. The attenuance increases through the visible range of the spectrum with an apparent maximum at ~1050 nm. The color changes are reversible, and the initial spectrum of the bleached film can be recovered by stepping the potential back to 0.0 V (SSCE) with a switching time on the order of tens of seconds.

Figure 4 displays the attenuance at 820 nm plotted versus applied potential for different film thicknesses, showing that the attenuance is proportional to the film thickness. Profilometry measurements show the thicknesses of the films are 16, 28, and 44 μm with variations in film thickness as large as ±10 μm. These films are therefore significantly thicker than those studied previously.[10] In some experiments, thinner films were prepared to examine the response at wavelengths close to the fundamental

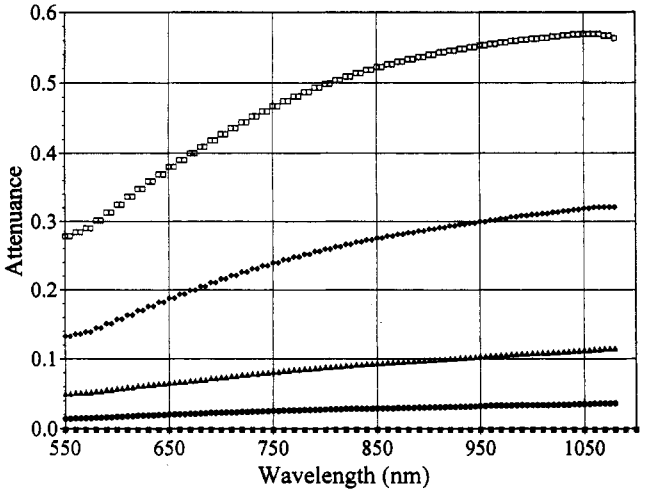

Figure 3. Attenuance spectra for a TiO_2 electrode in 0.1 M Na_2SO_4 at pH 2 as a function of electrode potential (SSCE): −1.0 V (open squares), −0.7 V (diamonds), −0.6 (triangles), −0.5 V (circles), and 0.0 V (filled squares) reference.

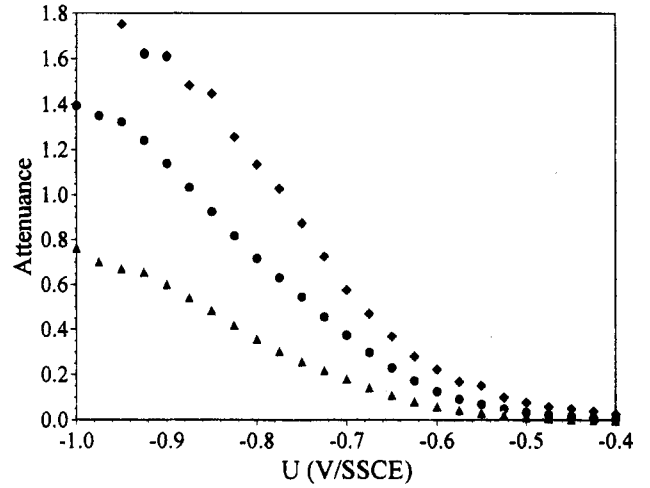

Figure 4. Attenuance difference at 820 nm versus applied potential for TiO_2 electrodes with different film thicknesses: triangles, 16 μm; circles, 28 μm; diamonds, 44 μm. Each curve represents an average from three samples, and for each thickness the scatter was typically less than 10%. Other experimental conditions are as given in Figure 3a.

absorption edge. In these experiments we observed a blue shift in the apparent fundamental absorption edge as the potential is shifted in the negative direction, in agreement with previous studies.[10] As can be seen in Figure 2a, the strong attenuance from these films can give rise to large errors in the attenuance difference spectra, especially at short wavelengths. As a result, detailed analysis of the observed blue shift is very difficult in these films.

An electron paramagnetic resonance (EPR) spectrum of electrochemically reduced TiO_2 particles recorded at 77 K is given in Figure 5. At this temperature a broad absorption is observed with $g = 1.903$. An EPR signal was observed only if the TiO_2 film was first electrochemically reduced under these experimental conditions.

Figure 6 shows a plot of the reoxidation charge versus the attenuance of the film. The attenuance data were recorded at the negative scan limit of the cyclic voltammogram, and the reoxidation charge was calculated by integration of the corresponding anodic peak. This plot shows that the attenuance of the film is directly correlated to the charge involved in the process.

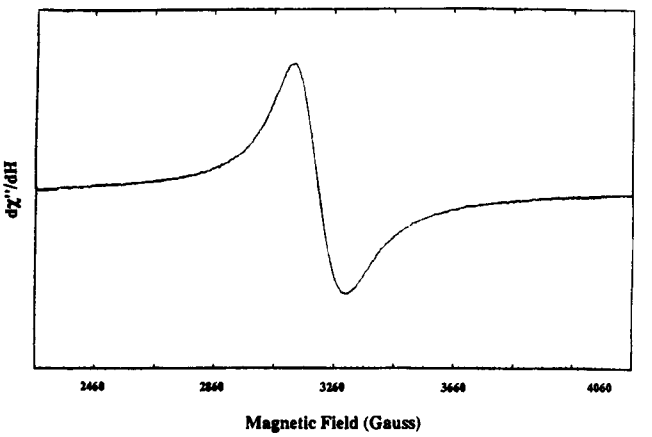

Figure 5. Electron paramagnetic resonance spectra of electrochemically reduced TiO_2 at 77 K. The single absorbance observed at $g = 1.903$ is assigned to Ti(III) species.

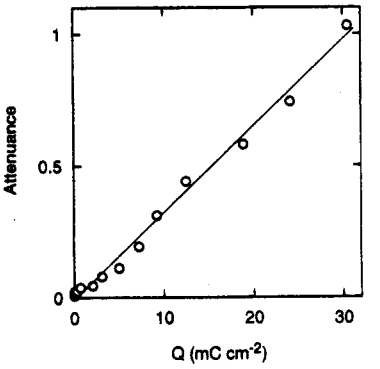

Figure 6. Charge under the anodic peak plotted against the attenuance as a function of the negative scan limit in the range −0.4 to −1.0 V (SSCE). Other experimental conditions are as given in Figure 8.

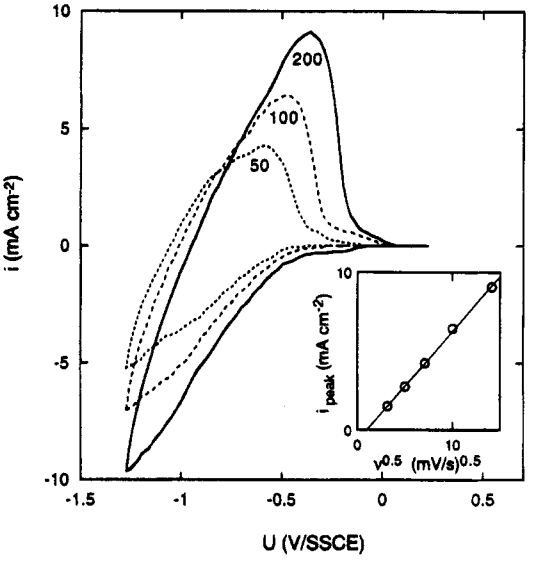

Figure 7. Cyclic voltammograms for a TiO_2 electrode in 0.1 M Na_2SO_4 at pH 2 as a function of scan rate. The inset displays the square root of the scan rate, ν, plotted versus the peak anodic current.

Figure 7 shows typical voltammograms for a TiO_2 film as a function of scan rate. At positive potentials the anodic current is very small, less than 1 μA cm^{-2} at 0.5 V (SSCE). On scanning the potential more negative the cathodic current increases steadily, and if the potential is scanned more negative than −0.4 V, an anodic peak is observed on the reverse scan. This peak is not observed in the voltammogram for the conductive glass substrate in the same solution. The inset shows

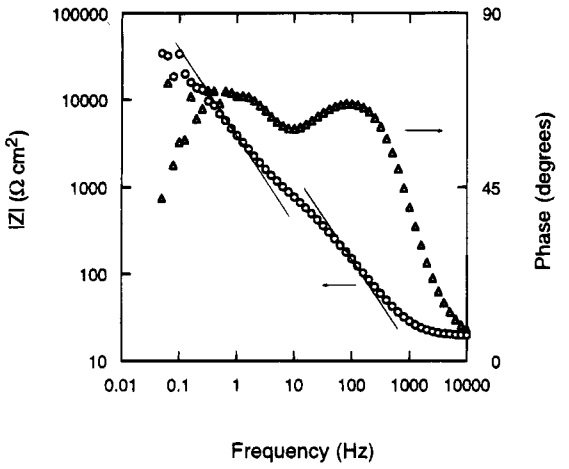

Figure 8. Magnitude and phase of the impedance of a TiO_2 electrode in 0.1 M Na_2SO_4 at pH 2 at 0.0 V (SSCE). The straight lines correspond to slopes of −1.0.

that the peak anodic current is proportional to the square root of the scan rate.

Electrochemical impedance spectroscopy has been used to analyze the potential distribution in the TiO_2 electrodes. Figure 8 shows a typical Bode plot for a TiO_2 film at 0.5 V (SSCE) in 0.1 M Na_2SO_4 buffered to pH 2. This figure reveals two capacitive regions with time constants of about 100 and 1 Hz. The origins of these two time constants can be seen from Mott−Schottky plots for the TiO_2 films and the conducting glass substrate derived from the parallel capacitance and shown in Figure 9, a and b, respectively. This representation is used for convenience and is not meant to imply that the Mott−Schottky relation holds for the TiO_2 films. The Mott−Schottky plots for the conducting glass substrate in the same solution show a linear region between 0.0 and 1.0 V (SSCE) and a much smaller degree of frequency dispersion than seen for the TiO_2 films. The high-frequency curves of the two plots are almost identical, demonstrating that at high frequency the total impedance of the TiO_2 films is dominated by the impedance of the conducting glass substrate which is partially exposed to the electrolyte. On decreasing the frequency, the capacitance of TiO_2 films begins to contribute to the total impedance of the TiO_2 electrode, resulting in the large-frequency dispersion in the Mott−Schottky plots. As a result, the higher frequency time constant in the Bode plot is due to the conducting glass substrate and the lower frequency time constant is due to the TiO_2 film.

Discussion

Structurally, the TiO_2 films are highly porous and are comprised of an interconnected network of approximately 25 nm diameter particles. The photoaction spectrum displays a small but significant sub-band gap response indicative of intra-band gap states.[24] The films are electrochromic and turn a uniform black color at potentials more negative than −0.4 V (SSCE). The attenuance increases as the potential is scanned in the negative direction, as shown in Figure 4, and reaches a plateau that is dependent on the film thickness, showing that the coloration occurs throughout the film. In thinner films, the apparent absorption edge shifts to higher energy with negative applied bias, as has been described previously.[10]

The appearance of a dark blue-black color on heated, irradiated, or electrochemically reduced titania materials is extremely well documented over the past several decades.[10,25] The absorption spectra are generally broad and display maxima in the visible or infrared region. The color change has been generally attributed to Ti(III) species, and there now exists a

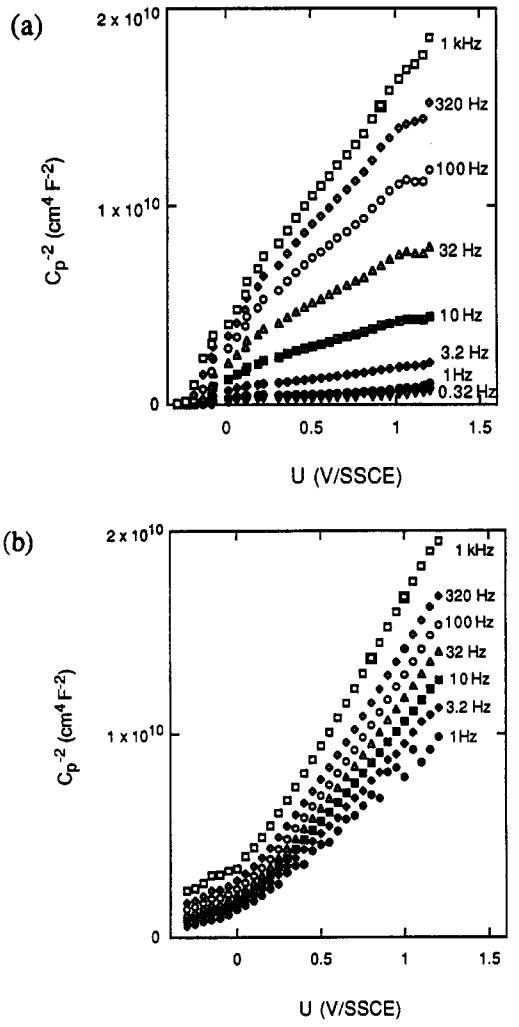

Figure 9. Mott−Schottky plots in 0.1 M Na_2SO_4 at pH 2 as a function of frequency. Panel (a) is from a TiO_2 electrode and (b) for the conducting tin oxide substrate alone. The frequencies are indicated on the plots.

large body of spectroscopic evidence to support this assignment. Perhaps the most detailed studies were performed by Von Hippel and co-workers, who explored the optical properties of single-crystal rutile materials. At temperatures above 900 °C the absorption increased through the visible and beyond 4 μm and was assigned to free electrons in a 3d conduction band.[25b] Extensive reduction of the crystal resulted in a room temperature discoloration with an absorption maximum at 1500 nm assigned to Ti(III) species in various surroundings.[25b] Therefore, the attenuance data reported here for porous nanocrystalline TiO_2 films support the presence of Ti(III) species. The high attenuance seen at negative potentials indicates that there is a very high density of these states. Further evidence for the presence of Ti(III) species is the appearance of an EPR absorption on electrochemically reduced films. The g factor of 1.903 is in good agreement with results from other titania materials excited with band gap light where similar spectra were obtained and assigned to Ti(III) species.[26] To our knowledge, this data represents the first observation by EPR that electrochemical reduction of TiO_2 leads to the formation of Ti(III) species.

The presence of free conduction band electrons at the surface in an accumulation layer may also give rise to color changes at negative potentials.[10] The potential dependence of the light scattering is unknown, and we are therefore only able to report attenuance spectra. However, the apparent maximum observed at ~1050 nm would suggest the presence of trapped electrons

although it is difficult to rule out the possibility that an underlying contribution from free carriers is also present. The absorption maximum from Ti(III) species is known to be critically dependent on processing conditions; a large variation in absorption maximum, optical cross section, and full width at half-maximum have been reported in the literature.[25] The nanostructured TiO_2 films studied here are inherently heterogeneous, and a distribution of Ti(III) species with broad overlapping absorption spectra is expected. Therefore, the relative contribution of free and trapped carriers to the attenuance spectra cannot be deconvoluted unless the potential dependencies of these terms are known.

In addition to the coloration of the films at negative potentials, a blue shift in the apparent fundamental absorption is observed.[10] Similar shifts in the absorption edge upon injection of negative charges have been observed, and a variety of mechanisms have been proposed to explain the phenomena. The underlying physics responsible for the shift remain unknown and a point of controversy in the literature.[27] In the accumulation layer model the blue shift can be explained by filling of conduction band states so that subsequent optical absorption from the valence band occurs to more energetic states in the conduction band.[28] For the band edge unpinning model, a blue shift could be explained by the presence of intraband states; at positive potentials valence band electrons are excited into these states whereas at negative potentials the states are filled, resulting in excitation to higher energy levels. Since the blue shift is observed at energies close to the fundamental absorption edge, this would suggest that these states are located near the conduction band edge. As a result, the observed blue shift does not yield conclusive evidence for band edge unpinning or the presence of an accumulation layer.

The black coloration of the porous nanocrystalline films is proportional to the film thickness which demonstrates that coloration occurs throughout the film and is not limited to the outer part of the film. This suggests that, in the absence of any *iR* drop, the internal surface of the film is at the solution potential. If the internal surface of the films is an equipotential surface, then any potential drop will be limited by the particle size and not the film thickness. The coloration associated with these films at negative potentials is attributed to Ti(III) species as described above, and there are at least two possible mechanisms for this process. In the first mechanism, conduction band electrons may be trapped directly on Ti(IV) sites. Due to the small particle size and the high surface-to-volume ratio, there is expected to be a high density of nonstoichiometric lattice sites where this process can occur. In the second mechanism, Ti(III) species may be generated indirectly by hydrogen intercalation. Adsorbed hydrogen atoms, generated by proton reduction, either can recombine to form molecular hydrogen or can be intercalated into the TiO_2 lattice. Reversible hydrogen intercalation is well-known for many metal oxide systems including single-crystal rutile.[29] Electrochemical loading of rutile crystals with hydrogen results in a surface layer with a characteristic blue-black color, and reduction in hydrogen gas is a well-known means of doping TiO_2 crystals.[30,31] On the basis of the experimental data reported here, it is not possible to differentiate between the two mechanisms.

As described in the Introduction, conventional models for interpretation of the potential dependence of the current or capacitance are not expected to be applicable for these porous materials. In these films the maximum band bending under depletion conditions can be estimated by calculating the depletion layer width for a 25 nm particle diameter and assuming $N_D = 10^{17}$ cm^{-3} and a relative permittivity of 173.[32] With these assumptions, the Albery–Bartlett model predicts the particle will be fully depleted at a band bending of about 0.6 meV.[12] Consequently, a cathodic current proportional to the surface electron concentration with a 60 mV/decade dependence (weak depletion) is not expected. For all of the experiments reported here, no exponential dependence of the current on applied potential was observed. We can also analyze the potential distribution for the formation of an accumulation layer. In this case, the excess free electron concentration in the accumulation layer is expected to increase by an order of magnitude for a 120 mV increase in the band bending.[15] Assuming that the reoxidation charge recorded on cycling the potential is equivalent to the total charge stored in the accumulation layer at negative bias, then a plot of the logarithm of the anodic charge versus applied potential should give a slope of 120 mV/decade. From our results we observe a slope of about 360 mV/decade, providing further evidence that a significant fraction of the applied potential is dropped over the Helmholtz layer due to unpinning of the band edges. The reduction of the Ti(IV) species in the TiO_2 films observed by EPR and attenuance measurements results in additional charge stored in the interface region which unpins the band edges since the Helmholtz layer has to accommodate the extra charge. The voltage change in the Helmholtz layer due to surface states can be estimated from

$$\Delta U_H = eN_{ss}/C_H \qquad (2)$$

where N_{ss} is the surface state density. Taking a density of interface states of 10^{14} cm^{-2} and the capacitance of the Helmholtz layer of 10 μF cm^{-2}, then the additional potential drop in the double layer can be as high as 1.6 V.[11]

The impedance measurements show that the high-frequency response is dominated by the conducting glass substrate whereas at low frequencies a contribution from the TiO_2 films is clearly seen. As the potential is shifted in the positive direction, less than 1 mV can be sustained in a depletion layer due to the small particle size.[12] However, as the potential is further increased, we would expect the TiO_2 particles to become fully depleted of electrons and behave as a dielectric between the conducting glass substrate and the solution. In this case the capacitance associated with each particle would be given by $C \approx \epsilon\epsilon_0/r$, where r is the particle radius. As a result, the capacitance of the TiO_2 film is expected to be independent of potential, consistent with impedance measurements where it was found that the low-frequency capacitance becomes nearly independent of potential. Since both the conducting glass substrate and the TiO_2 film are in contact with the solution, it may be expected that only a fraction of the applied potential is dropped across the TiO_2 film. The impedance measurements confirm that there is a potential drop across the film; however, the potential drop is expected to be larger in the individual particles closer to the conductive glass substrate due to the resistance associated with the nanocrystalline film. Even if the potential drop across an individual particle is only a few millivolts, the average field would be sufficient to provide a driving force for electron collection during cell operation.

Conclusions

The potential distribution at porous nanocrystalline films is highly complex due to the three-dimensional structure and the fact that both the film and the conducting glass substrate are in contact with the electrolyte. The optical and electrochemical response of these films is consistent with a model where coloration is associated with electrons trapped in Ti(IV) states which results in unpinning of the band edges. The presence of

these states is observed in the sub-band gap response of the photocurrent action spectra, cyclic voltammetry, EPR measurements, and attenuance spectra. The internal surface of the film is at the solution potential, and the coloration occurs uniformly throughout the film. The reversible coloration is directly correlated to the charge stored in the trap states, indicating that the states observed in optical and electrochemical measurements are the same.

Finally, we note that many aspects of the interpretation presented here are not special features of nanostructured electrodes but are well established in the conventional photoelectrochemical literature. The reversible trapping of electrons at surface sites has been reported for many n-type compound semiconductors at sufficiently negative potentials. Examples include InP,[33] ZnO,[34] and CdS[35] in aqueous solution. In these cases, the surface of the semiconductor is reduced, resulting in the formation a lower oxidation state which can be reoxidized on the reverse scan giving rise to an anodic current. Of particular relevance here is the work related to coloration and electrochemical doping of single-crystal rutile electrodes where similar shifts in the band edges have been observed.[29,36]

Acknowledgment. This work was supported by the National Renewable Energy Laboratory under Subcontract XAD-3-12114-04.

References and Notes

(1) Meyer, G. J.; Searson, P. C. *Interface* **1993**, *2*, 23.

(2) (a) Vinodgopal, K.; Hotchandani, S.; Kamat, P. V. *J. Phys. Chem.* **1993**, *97*, 9040. (b) Vinodgopal, K.; Stafford, U.; Gray, K. A.; Kamat, P. V. *J. Phys. Chem.* **1994**, *98*, 6797.

(3) (a) Bedja, I.; Hotchandani, S.; Carpentier, R.; Vinodgopal, K.; Kamat, P. V. *Thin Solid Films* **1994**, *247*, 195. (b) Bedja, I.; Hotchandani, S.; Fessenden, R. W.; Kamat, P. V. *Langmuir* **1994**, *10*, 17. (c) Hagfeldt, A.; Vlachopoulos, N.; Grätzel, M. *J. Electrochem. Soc.* **1994**, *141*, L82. (d) Vinodgopal, K.; Kamat, P. V. *Environ. Sci. Technol.* **1995**, *29*, 841.

(4) (a) O'Regan, B.; Grätzel, M. *Nature* **1991**, *353*, 737. (b) Kay, A.; Grätzel, M. *J. Phys. Chem.* **1993**, *97*, 6272. (c) Nazeeruddin, M. K.; Kay, A.; Rodicio, I.; Humphry-Baker, R.; Muller, E.; Liska, P.; Vlachopoulos, N.; Grätzel, M. *J. Am. Chem. Soc.* **1993**, *115*, 6382.

(5) (a) Heimer, T. A.; Bignozzi, C. A.; Meyer, G. J. *J. Phys. Chem.* **1993**, *97*, 11987. (b) Argazzi, R.; Bignozzi, C. A.; Heimer, T. A.; Castellano, F. N.; Meyer, G. J. *Inorg. Chem.* **1994**, *33*, 5741.

(6) (a) Bedja, I.; Hotchandani, S.; Carpentier, R.; Fessenden, R. W.; Kamat, P. V. *J. Appl. Phys.* **1994**, *75*, 5444. (b) Bedja, I.; Hotchandani, S.; Kamat, P. V. *J. Phys. Chem.* **1994**, *98*, 4133. (c) Liu, D.; Kamat, P. V. *J. Phys. Chem.* **1994**, *98*, 10769.

(7) Hodes, G.; Howell, I. D.; Peter, L. M. *J. Electrochem. Soc.* **1992**, *139*, 3136.

(8) Rothenberger, G.; Grätzel, M.; Fitzmaurice, D. *J. Phys. Chem.* **1992**, *96*, 5983.

(9) Sodergren, S.; Hagfeldt, A.; Olsson, J.; Lindquist, S.-E. *J. Phys. Chem.* **1994**, *98*, 5552.

(10) (a) Redmond, G.; Grätzel, M.; Fitzmaurice, D. *J. Phys. Chem.* **1993**, *97*, 6951. (b) Fitzmaurice, D. *Sol. Energy Mater.* **1994**, *32*, 289. (c) Enright, B.; Redmond, G.; Fitzmaurice, D. *J. Phys. Chem.* **1994**, *98*, 6195.

(11) Finklea, H. O. In *Semiconductor Electrodes*; Finklea, H. O., Ed.; Elsevier: Amsterdam, 1988.

(12) Albery, W. J.; Bartlett, P. N. *J. Electrochem. Soc.* **1984**, *131*, 315.

(13) (a) Many, A.; Goldstein, Y.; Groover, H. Z. *Semiconductor Surfaces*; Wiley & Sons: New York, 1965. (b) Morrison, S. R. *The Chemical Physics of Surfaces*; Plenum Press: New York, 1977.

(14) (a) Morrison, S. R. *Surf. Sci.* **1969**, *15*, 363. (b) Vanden Berghe, R. A. L.; Cardon, F.; Gomez, W. P. *Surf. Sci.* **1973**, *39*, 368. (c) Gerischer, H. *Electrochim. Acta* **1990**, *35*, 1677.

(15) (a) Dewald, J. F. *Bell Syst. Technol. J.* **1960**, *39*, 615. (b) Sze, S. M. *Physics of Semiconductor Devices*; Wiley: New York, 1981; pp 366–369.

(16) Seeger, K. *Semiconductor Physics: An Introduction*; Springer-Verlag: Berlin, 1982; pp 343–356.

(17) Chmiel, G.; Gerischer, H. *J. Phys. Chem.* **1990**, *94*, 1612 and references therein.

(18) Mettler, K. *Appl. Phys.* **1977**, *12*, 75.

(19) (a) Pond, S. F. *Surf. Sci.* **1973**, *37*, 596 and references therein. (b) Silberstein, R. P.; Lyden, J. K.; Tomkiewicz, M.; Pollak, F. H. *J. Vac. Sci. Technol.* **1981**, *19*, 406. (c) Tomkiewicz, M.; Lyden, J. K.; Silberstein, R. P.; Pollak, F. H. In *Photoeffects at Semiconductor–Electrolyte Interfaces*; ACS Symposium Series 146; Nozik, A. J., Ed.; American Chemical Society: Washington, DC, 1981; p 267.

(20) Eger, D.; Goldstein, Y. *Phys. Rev. B* **1979**, *19*, 1089.

(21) Bard, A. J.; Bocarsly, A. B.; Fan, F-R. E.; Walton, E. G.; Wrighton M. S. *J. Am. Chem. Soc.* **1980**, *102*, 3671.

(22) Wertz, J. E.; Bolton, J. R. *Electron Spin Resonance: Elementary Theory and Practical Application*; Chapman and Hall: London, 1986.

(23) Sheppard, N.; Willis, H. A.; Rigg, J. C. *Pure Appl. Chem.* **1985**, *57*, 105.

(24) (a) Pankove, J. I. *Optical Processes in Semiconductors*; Dover Publications; New York, 1971. (b) Mott, N. F.; Davis, E. A. *Electronic Processes in Non-Crystalline Materials:* Clarendon Press: Oxford, 1979.

(25) (a) Grant, F. A. *Rev. Mod. Phys.* **1959**, *31*, 646. (b) von Hippel, A.; Kalnjas, J.; Westphal, W. B. *J. Phys. Chem. Solids* **1962**, *23*, 779. (c) Balberg, I.; Braun, P.; Viehbock, F. P. *Sol. Energy Mater.* **1982**, *7*, 183. (d) Dimitrijevic, N. M.; Savic, D.; Micic, O. I.; Nozik, A. *J. J. Phys. Chem.* **1984**, *88*, 4278. (e) Kolle, U.; Moser, J.; Grätzel, M. *Inorg. Chem.* **1985**, *24*, 2253. (f) Rothenberger, G.; Moser, J.; Grätzel, M.; Serpone, N.; Sharma, D. K. *J. Am. Chem. Soc.* **1985**, *107*, 8054. (g) Kormann, C.; Bahnemann, D. W.; Hoffman, M. R. *J. Phys. Chem.* **1988**, *92*, 5196.

(26) (a) Huizinga, T.; Prins, R. *J. Phys. Chem.* **1981**, *85*, 2156. (b) Howe, R. F.; Grätzel, M. *J. Phys. Chem.* **1985**, *89*, 4495. (c) Howe, R. F.; Grätzel, M. *J. Phys. Chem.* **1987**, *91*, 3906. (d) Howe, R. F.; Grätzel, M. *J. Phys. Chem.* **1990**, *94*, 2566. (e) Micic, O. I.; Zhang, Y.; Cromack, K. R.; Trifunac, A. D.; Thurnauer, M. C. *J. Phys. Chem.* **1993**, *97*, 7277. (f) Micic, O. I.; Zhang, Y.; Cromack, K. R.; Trifunac, A. D.; Thurnauer, M. C. *J. Phys. Chem.* **1993**, *97*, 13284. (g) Castellano, F. N.; Stipkala, J. M.; Friedman, L. A.; Meyer, G. J. *Chem. Mater.* **1994**, *6*, 2123.

(27) (a) Henglein, A. *Topics in Current Chemistry*; Springer-Verlag: Berlin, 1988; pp 343–356 and references therein. (b) Wang, Y.; Herron, N. *J. Phys. Chem.* **1991**, *95*, 525 and references therein.

(28) Burstein, E. *Phys. Rev.* **1954**, *93*, 632.

(29) Schumacher, R. *Ber. Bunsen-Ges. Phys. Chem.* **1980**, *84*, 125.

(30) (a) Harris, L. A.; Schumacher, R. *J. Electrochem. Soc.* **1980**, *127*, 1186. (b) Harris, L. A.; Gerstner, M. E.; Wilson, R. H. *J. Electrochem. Soc.* **1979**, *126*, 850. (c) Chester, P. F.; Bradhurst, P. H. *Nature* **1963**, *149*, 1056.

(31) Cantao, M. P.; Cisneros, J. I.; Torresi, R. M. *J. Phys. Chem.* **1994**, *98*, 4865.

(32) (a) Boddy, P. J. *J. Electrochem. Soc.* **1968**, *115*, 199. (b) We note that there exists considerable literature uncertainty in the rutile TiO_2 dielectric constant. Reference 32a was chosen as a representitive value, and a different dielectric constant will quantitatively alter the magnitude of the maximum theoretical potential drop but will not effect the discussion here.

(33) (a) Uosaki, K.; Kita, H. *Sol. Energy Mater.* **1983**, *7*, 421. (b) Oskam, G.; Meulenkamp, E. A. *J. Electroanal. Chem.* **1992**, *326*, 213.

(34) de Wit, A. R.; Janssen, M. D.; Kelly, J. J. *Appl. Surf. Sci.* **1990**, *45*, 1.

(35) de Wit, A. R.; Kelly, J. J. *Ber. Bunsen-Ges. Phys. Chem.* **1991**, *95*, 670.

(36) (a) Gutierrez, C.; Salvador, P. *J. Electroanal. Chem.* **1982**, *138*, 457. (b) Ginley, D. S.; Knotek, M. L. *J. Electrochem. Soc.* **1979**, *126*, 2163.

JP951140B